Dielectric barrier plasma dynamics for active control of separated flows

Subrata Roy[a] and K. P. Singh
Computational Plasma Dynamics Laboratory, Mechanical Engineering, Kettering University, Flint, Michigan 48504

Datta V. Gaitonde
Computational Sciences Branch, Air Vehicles Directorate, Air Force Research Laboratory, Wright Patterson AFB, Ohio 45433

(Received 3 November 2005; accepted 21 February 2006; published online 20 March 2006)

The dynamics of separation mitigation with asymmetric dielectric barrier discharges is explored by considering the gas flow past a flat plate at an angle of attack. A self-consistent model utilizing motion of electrons, ions, and neutrals is employed to couple the electric force field to the momentum of the fluid. The charge separation and concomitant electric field yield a time-averaged body force which is oriented predominantly downstream, with a smaller transverse component towards the wall. This induces a wall-jet-like feature that effectively eliminates the separation bubble. The impact of several geometric and electrical operating parameters is elucidated. © *2006 American Institute of Physics*. [DOI: 10.1063/1.2187951]

Active flow control is vital to many practical applications. Examples include low-pressure turbines in propulsion,[1] external aerodynamics about an aircraft wing where an efficient passive[2] or active control[3] is important to mitigate performance deficiencies at off-design conditions. Specifically, plasma-based actuators exhibit several potential benefits in active flow control applications, including absence of moving parts, rapid on-off deployment, and attractive self-limiting characteristics. In recent years, experimental observations have shown the capability of dielectric barrier devices, operating at relatively low power levels, to suppress separation in a wide range of applications even at atmospheric pressures.[4,5] The discharge may be characterized as a transient microdischarge. The time scale for this discharge is smaller than microseconds and that for the neutral gas is in milliseconds. The present authors have developed a self-consistent multifluid model for volume[6] and surface[7,8] barrier discharges. The model described the interaction between the electric field and the fluid mixture comprised of ions, electrons, and neutrals under quiescent (no external flow) condition. In this letter, we utilize the methodology to study active separation control using asymmetric dielectric barrier plasma actuator. The configuration considered is a flat plate placed at an angle of attack in an oncoming stream of fluid. The separated region observed in the vicinity of the leading edge of the plate is then subjected to control with a suitably placed asymmetric single dielectric barrier plasma actuator. We solve the equations governing dynamics of electrons, ions, and fluid to obtain spatiotemporal profiles of electron density, ion density, electric potential, fluid density, and fluid velocity.

A typical electrode arrangement for such actuation devices is shown in Fig. 1 where the grounded electrode is surrounded by an insulator and a voltage fluctuating at rf is applied to the electrode exposed to the gas. Here, the working gas is helium at a bulk pressure and temperatures of 300 Torr and 300 K, respectively. Positive helium ions are formed through a process of direct and stepwise ionization, and dissociative recombination. The electric field $\mathbf{E}$ exerts a net force $q\mathbf{E}$ through the space charge (q)separated plasma within the dielectric barrier discharge (DBD). The parameters controlling such force are the applied voltage, frequency, dielectric characteristics, the asymmetric configuration of the electrodes, and the thickness of the exposed electrode. The effect of these parameters on separation control mechanism is also characterized in this letter.

The region simulated is 10 cm long and 5 cm high. The lower part of the domain consists of a 0.1 cm thick insulator with dielectric constant $\epsilon_d = a\epsilon_0$ while the upper part is filled with inert helium gas of $\epsilon_f = 1.0055\epsilon_0$, where ϵ_0 is permittivity of the free space. The embedded electrode is grounded and a sinusoidal voltage $\phi = \phi_0 \sin(2\pi ft)$ is applied to the exposed electrode. The frequency of excitation is fixed at $f = 5$ kHz while the influence of different amplitudes, ϕ_0, is also explored.

The drift-diffusion form of continuity and Poisson's equations for the electrons and ions are solved with the fluid momentum and continuity equations as described in (Ref. 7 and 8). The bulk density of the helium is taken to be 1.79×10^{-4} g/cm^3, and the viscosity is assumed to be 1.9 poise. The self-consistent formulation is solved using a variational formulation based on Galerkin finite-element method[9] to obtain electron and ion density, electric potential, neutral velocity, and density.

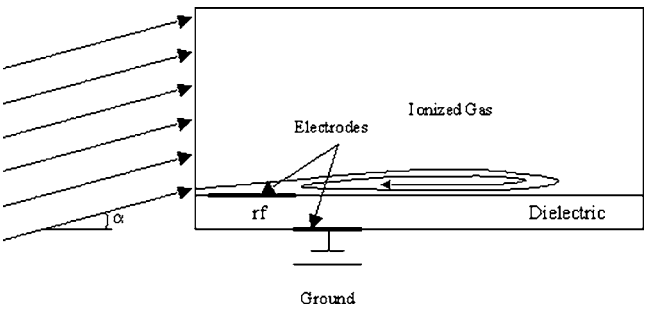

FIG. 1. Schematic of an asymmetric single dielectric barrier plasma actuator with an incident gas flow angle α.

[a]Author to whom correspondence should be addressed; electronic mail: sroy@kettering.edu

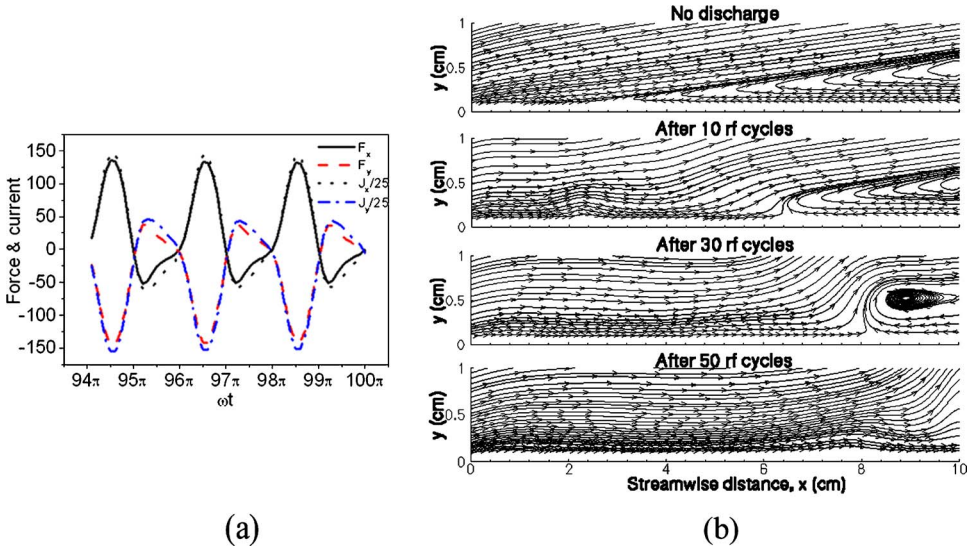

FIG. 2. (Color online) (a) The force per unit volume $e(n_i-n_e)\mathbf{E}$ (dyn/cm^3) and currents components as function of ωt at $x=1.75$ cm and $y=0.25$ cm. (b) Streamlines and vectors of gas velocity at the end of 1 s, 10 cycles, 30 cycles, and 50 cycles.

For all cases reported here, the rf electrode extends from $x=0.3$ to 1.5 cm at $y=0.1$ cm, the grounded electrode is from $x=1.48$ to 2.75 cm at $y=0$, with a 0.02 cm overlap between electrodes along the x axis. The initial velocity components u_0 (along the x direction) and v_0 (along the y direction) are 1000 and 175 cm/s, respectively, corresponding to an angle of attack (α) of approximately 10°. The no-slip condition is assumed for the gas neutrals at the dielectric and exposed electrode surfaces and the velocity at the left boundary of upper domain is set to the freestream condition at all times. Homogeneous Neumann conditions are applied to the upper edge of the domain. For the charge equations, the total current continuity is ensured across the dielectric interface; i.e., at this location, conduction, convection, and displacement currents in the gas are balanced with the displacement current in the dielectric.

The present study reports a parametric study in which applied rf voltage ϕ_0, initial plasma density n_0, dielectric constant a, and rf electrode shape are varied. Unless otherwise stated, $n_0=10^{10}/\text{cm}^3$, $a=3.5$, $\phi_0=400$ V, and rf electrode thickness is negligible. Since the gas is preionized, a reasonably small rf potential is assumed sufficient to maintain the discharge.

The electrons are repelled by the insulated electrode and by the exposed electrode during most of the positive and the negative part of the rf voltage, respectively. The local imbalance arising from the disparate mobilities of the ions and electrons results in a time-varying charge separation distribution and establishment of a consistent electric field. The generated electric field restricts movement of electrons away from the domain. At all phases in the cycle, the peak magnitude of the force is located downstream of the rf electrode. Figure 2(a) plots the calculated forces per unit volume $e(n_i-n_e)\mathbf{E}$, where the electric field $\mathbf{E}=-\nabla\phi$, and the discharge current as function of ωt at $x=1.75$ cm and $y=0.25$ cm. Although the x component of the force takes both positive and negative values during positive and negative parts of the cycle, respectively, its magnitude during the former phase is nearly three times larger than in the latter. Magnitude of force components is the highest around positive peak of the cycle and almost zero at the end of the cycle. The time average of the force at this point is oriented in the positive x and negative y direction. Consequently, collision effects ensure that the dominant neutral species experience an accelerating body force downstream and towards the dielectric surface. Since fluid cannot penetrate the dielectric, it is turned parallel to the surface of the dielectric. The net effect as discussed further below is therefore a gradual mitigation of flow separation. Ensuring the proper ratio between accelerating and retarding forces is the key to successful application of DBD for actuating effect at higher neutral gas speeds.

The effect of DBD is highlighted by considering the flow field. The initial field, without plasma actuator, is shown in the first frame of Fig. 2(b), which depicts the stream traces of neutral velocity at 1 s (roughly 1000 times the characteristic flow time scale) after initiation of the flow. A separation bubble develops over the exposed surface degrading performance due to increased drag and turbulent flow structures. When the plasma actuator is switched on, a highly transient process is initiated as shown in the last three frames of Fig. 2(b), which depicts stream traces of neutral velocity after 10, 30, and 50 cycles, respectively. The attachment process downstream of the rf electrode progresses successively: the attachment point is at 6.5 cm after 10 cycles, moving to 8 cm after 30 cycles and finally beyond the computational domain after 50 cycles. The transfer of momentum results in a near-wall energized flow of neutrals, altering the dynamics of the inertial and adverse pressure gradient terms to eliminate the separation bubble. Since the neutral density is nearly 10^7 times higher than that of the plasma, therefore, quick acting controls may be limited in high speed flows and inertia ef-

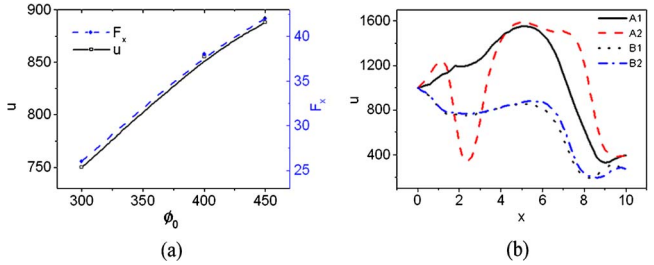

FIG. 3. (Color online) (a) Velocity u (cm/s) and the force F_x (dyn/cm^3) as a function of rf voltage ϕ_0 (in volts). (b) Gas velocity u as a function of x in cm. Different lines are at $y=0.25$ cm for initial plasma density $5\times10^{10}/\text{cm}^3$ (A1), $1\times10^{11}/\text{cm}^3$ (A2), dielectric constant $\epsilon=7$ (B1), and $\epsilon=10.5$ (B2).

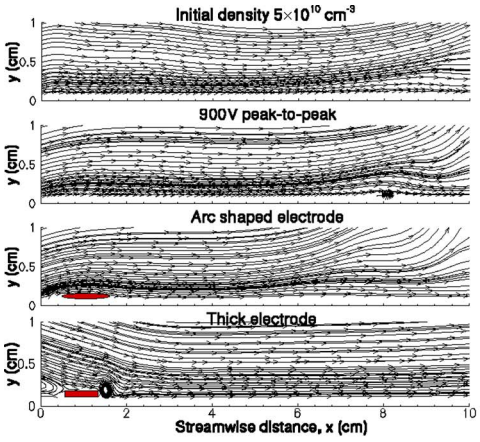

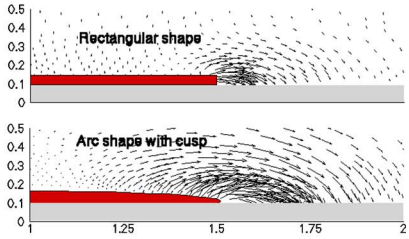

FIG. 4. (Color online) (a) Streamlines and vectors of gas velocity for the cases with $5\times10^{10}/\mathrm{cm}^3$, $\phi_0=450$ V, finite thickness (0.05 cm) and arc shape rf electrode. (b) Time-averaged force distribution showing the effect of electrode radius. x and y are in cm.

fects are reflected in the response time taken to attach the flow over full length of the dielectric.

The effect of excitation amplitude was explored by considering ϕ_0 values of 450, 400, and 300 V. For these three values, the correlation between the streamwise component of velocity and body force is highlighted in Fig. 3(a) which plots them against amplitude of excitation. The magnitudes of the two quantities are correlated with applied voltage in showing the relationship $G\sim C\phi_0^m$ (cf. Ref. 5). For $G\equiv u$ in cm/s and $\phi_0$in volts we determined $C=77.0$ and $m=0.4$, while for $G\equiv F_x$, $C=0.03$ and $m=1.2$. This indicates that due to viscous drag even as the force increases, the resulting imparted fluid velocity does not keep growing indefinitely and may reach a point of diminishing return beyond certain optimum electrical input. For all cases, the positive peak of the force occurs near $x=1.75$ cm, i.e., just downstream of the trailing edge of the exposed electrode, while negative peak is observed at $x\sim3$ cm. As ϕ_0 increases by 50%, the streamwise force increases by a commensurate amount. The magnitudes of both the components of the force decrease sharply with y and are negligible beyond $x=4$ cm.

The effect of dielectric constant and initial plasma density is explored in Fig. 3(b), which shows streamwise neutral velocity for initial plasma density 5×10^{10} cm^{-3} (curve A1) and 10^{11} cm^{-3} (A2), and dielectric constant $a=7$ (B1) and 10.5 (B2), respectively. The higher value of initial density results in larger charge separation and hence higher generated electrostatic field. Consistently, the larger force $e(n_i-n_e)\mathbf{E}$ yields more energetic plasma and neutral velocities. Variation of dielectric constant does not have a significant effect on the velocities. A summary comparison of performance of a single pair actuator under four different design conditions is plotted in Fig. 4(a). Unless otherwise stated for these cases $n_0=5\times10^{10}/\mathrm{cm}^3$, $\phi_0=450$ V. During simulations it was found (not shown) that the flow is smoother for plasma density $5\times10^{10}/\mathrm{cm}^3$ than those for plasma densities $10^{10}/\mathrm{cm}^3$ and $10^{11}/\mathrm{cm}^3$. The flow is best attached to the surface in the case of arcshape rf electrode case which is due to increase in the x component of the force $e(n_i-n_e)\mathbf{E}$ as observed earlier. Figure 4(b) demonstrates the effect of electrode radius of curvature. As compared to the sharp corner raised electrode, the cycle averaged force magnitude nearly doubles for an arc shaped electrode with a small cusp at the tip. This confirms the experimental observation reported in Ref. 5. It is important to identify that in air, negative ions and metastable species may be present. However, the essential characteristics of the electric body force development and its distribution, and the evolution of separation mitigation will be quite similar to that described here.

In conclusion, the impact of momentum transfer and the consequent enhancement of near-wall neutral velocity on the flow structure have been explored. A net streamwise-oriented force is generated, which acts on plasma predominantly in the region downstream of the rf electrode. Momentum transfer from charged particles to the neutrals results in an energized near-wall flow, facilitating the elimination of a separation bubble. Several parameters of the actuator affect separation control characteristics, including the length of the rf electrode, its shape and location relative to the embedded electrode, and properties of the dielectric, rf voltage characteristics and initial plasma density. Simulation confirms the experimental observation that the force magnitude increases with decreasing radius of electrode. However, scalability to large systems remains a concern since induced force and fluid velocity do not increase indefinitely.

In real applications, air may be used and water or water vapor may be present. This will affect the chemistry of ions formation. The separation can be controlled in either case due to the directional body force. A thin insulating layer over the upper electrode may be also used to increase the durability of the electrode. Optimization methodologies are necessary to generate such effective designs.

This work is partially supported by Air Force Research Laboratory Contract No. F33615-98-D-3210 and support from the AFOSR Grant No. FA9550-05-1-0074 (Monitor: John Schmisseur).

[1]R. E. Mayle, J. Turbomach. **113**, 509 (1991).
[2]K. W. Van Treuren, T. Simon, M. von Koller, A. R. Byerley, J. W. Baughn, and R. B. Rivir, J. Turbomach. **124**, 100 (2002).
[3]J. P. Bons, R. Sondergard, and R. B. Rivir, J. Turbomach. **123**, 198 (2001).
[4]J. R. Roth, Phys. Plasmas **10**, 2117 (2003).
[5]C. L. Enloe, T. E. McLaughlin, R. D. VanDyken, K. D. Kachner, E. J. Jumper, T. C. Corke, M. Post, and O. Haddad, AIAA J. **42**, 595 (2004).
[6]S. Roy and D. Gaitonde, J. Appl. Phys. **96**, 2476 (2004).
[7]S. Roy, Appl. Phys. Lett. **86**, 101502 (2005).
[8]K. P. Singh and S. Roy, J. Appl. Phys. **98**, 083303 (2005).
[9]S. Roy, B. P. Pandey, J. Poggie, and D. V. Gaitonde, Phys. Plasmas **10**, 2578 (2003).